

Article

Sensitive Electrochemical Detection of 4-Nitrophenol with PEDOT:PSS Modified Pt NPs-Embedded PPy-CB@ZnO Nanocomposites

Mohd Faisal^{1,2}, Md. Mahmud Alam³ , Jahir Ahmed¹, Abdullah M. Asiri^{3,4} , Mohammed Jalalah^{1,5} ,
Raja Saad Alruwais⁶, Mohammed M. Rahman^{3,4,*}  and Farid A. Harraz^{1,7,*} 

¹ Promising Centre for Sensors and Electronic Devices (PCSED), Advanced Materials and Nano-Research Centre, Najran University, P.O. Box 1988, Najran 11001, Saudi Arabia

² Department of Chemistry, Faculty of Science and Arts, Najran University, Najran 11001, Saudi Arabia

³ Center of Excellence for Advanced Materials Research (CEAMR), King Abdulaziz University, Jeddah 21589, Saudi Arabia

⁴ Department of Chemistry, Faculty of Science, King Abdulaziz University, Jeddah 21589, Saudi Arabia

⁵ Department of Electrical Engineering, College of Engineering, Najran University, Najran 11001, Saudi Arabia

⁶ Chemistry Department, Faculty of Science and Humanities, Shaqra University, Dawadmi 17472, Saudi Arabia

⁷ Department of Chemistry, Faculty of Science and Arts at Sharurah, Najran University, Najran 11001, Saudi Arabia

* Correspondence: mmrahman@kau.edu.sa (M.M.R.); faharraz@nu.edu.sa (F.A.H.)

Abstract: In this study, a selective 4-nitrophenol (4-NP) sensor was developed onto a glassy carbon electrode (GCE) as an electron-sensing substrate, which decorated with sol-gel, prepared Pt nanoparticles- (NPs) embedded polypyrrole-carbon black (PPy-CB)/ZnO nanocomposites (NCs) using differential pulse voltammetry. Characterizations of the NCs were performed using Field Emission Scanning Electron Microscopy (FESEM), Energy-Dispersive Spectroscopy (EDS), X-ray Photoelectron Spectroscopy (XPS), Ultraviolet-visible Spectroscopy (UV-vis), Fourier Transform Infrared Spectroscopy (FTIR), High Resolution Transmission Electron Microscopy (HRTEM), and X-ray Diffraction Analysis (XRD). The GCE modified by conducting coating binders [poly(3,4-ethylenedioxythiophene) polystyrene sulfonate; PEDOT:PSS] based on Pt NPs/PPy-CB/ZnO NCs functioned as the working electrode and showed selectivity toward 4-NP in a phosphate buffer medium at pH 7.0. Our analysis of 4-NP showed the linearity from 1.5 to 40.5 μM , which was identified as the linear detection range (LDR). A current versus concentration plot was formed and showed a regression co-efficient R^2 of 0.9917, which can be expressed by $i_p(\mu\text{A}) = 0.2493C(\mu\text{M}) + 15.694$. The 4-NP sensor sensitivity was calculated using the slope of the LDR, considering the surface area of the GCE (0.0316 cm^2). The sensitivity was calculated as $7.8892\ \mu\text{A}\ \mu\text{M}^{-1}\ \text{cm}^{-2}$. The LOD (limit of detection) of the 4-NP was calculated as $1.25 \pm 0.06\ \mu\text{M}$, which was calculated from $3xSD/\sigma$ (SD: Standard deviation of blank response; σ : Slope of the calibration curve). Limit of quantification (LOQ) is also calculated as $3.79\ \mu\text{M}$ from $LOQ = 10xLOD/3.3$. Sensor parameters such as reproducibility, response time, and analyzing stability were outstanding. Therefore, this novel approach can be broadly used to safely fabricate selective 4-NP sensors based on nanoparticle-decorated nanocomposite materials in environmental measurement.

Keywords: Pt-NPs-embedded PPy-CB/ZnO nanocomposites; 4-nitrophenol detection; differential pulse voltammetry; glassy carbon electrode; environmental safety



Citation: Faisal, M.; Alam, M.M.; Ahmed, J.; Asiri, A.M.; Jalalah, M.; Alruwais, R.S.; Rahman, M.M.; Harraz, F.A. Sensitive Electrochemical Detection of 4-Nitrophenol with PEDOT:PSS Modified Pt NPs-Embedded PPy-CB@ZnO Nanocomposites. *Biosensors* **2022**, *12*, 990. <https://doi.org/10.3390/bios12110990>

Received: 25 September 2022

Accepted: 6 November 2022

Published: 8 November 2022

Publisher's Note: MDPI stays neutral with regard to jurisdictional claims in published maps and institutional affiliations.



Copyright: © 2022 by the authors. Licensee MDPI, Basel, Switzerland. This article is an open access article distributed under the terms and conditions of the Creative Commons Attribution (CC BY) license (<https://creativecommons.org/licenses/by/4.0/>).

1. Introduction

Generally, 4-nitrophenol (4-NP), also known as para-nitro-phenol, is an organic pollutant. It is acidic in nature and moderately soluble in water. Due to its industrial importance, it has diversified industrial, pharmaceutical, and agricultural applications and is used in medicine, dyes, insecticides, herbicides, and fungicides [1]. For widespread industrial

activities, thousands of tons of industrial waste are released into the environment, which has hazardous impacts on soils and ground and underground water. Subsequently, there is a great possibility of transferring it into human and animal bodies through the food chain [2]. The numerous physiological syndromes such as cyanosis, nausea, drowsiness, and headaches may appear in humans by the acute ingestion or inhalation of 4-NP. Contact of 4-NP with human eyes and skin may cause irritation [3,4]. Based on the toxicity of 4-NP, long-term exposure can cause irreversible damage to the liver, kidneys, and nervous system [5,6]. Therefore, 0.34 mg/cm³ 4-NP is considered the upper limit in potable water [7]. Considering the hazardous effects of 4-NP, it is important to detect and quantify various water sources in soil and the environment. Detection techniques such as gas chromatography (GC-MS), surface-enhanced Raman spectroscopy (SERS), liquid chromatography (LC) coupled with mass spectrometry (LC-MS), capillary electrophoresis, fluorescence, and high-performance liquid chromatography (HPLC) are widely used for these purposes [8]. These technologies are limited by their costly equipment, operating complications, and need for special arrangements and facilities. Therefore, these methods are suitable for clinical diagnosis but not for outdoor analysis. Thus, we propose a cost-effective and portable measuring system which is easy to use and necessary for the in situ diagnosis of the environmental unfriendly 4-NP. Electrochemical methods, including cyclic voltammetry (CV), differential-pulse voltammetry (DPV), linear-sweep voltammetry (LSV), and current-voltage (I-V) relation, are extensively utilized by researchers to develop potential detecting chemicals and measuring systems or devices. Due to the poor electron transfer rate on the working electrode of these methods, good outcomes are not obtained in this regard. Therefore, the working electrode surfaces in these methods are modified by coating them with sensing substrates (such as metal oxide nanoparticles or organometallic nanocomposites) to obtain enhanced performance [9–12]. Thus, the aim of this study is to develop an electrochemical sensor applying differential pulse voltammetry (DPV) to analyze 4-NP in a conductive aqueous medium. Metal oxides such as Cu₂O NPs [13], ZnBi₃₈O₆₀ nanobundles [14], doped metal oxide nanocomposites [15], and ZnO-Au NPs [10] have been used to modify the working electrode of the 4-NP sensor via the DPV method. On the other hand, various organometallic nanocomposites such as GCEs modified by graphene-chitosan (GR-CS) [16] and Ag NP-chitosan composites [17], have been studied for the detection of 4-NP by applying the DPV method. In addition, poly(methyl orange) has also been studied to analyze 4-NP [18]. Therefore, polymer nanocomposites decorated with metal oxides have been applied to detect 4-NP in an aqueous phase.

In this study, a polymer (polypyrrole) was composited with carbon black and doped with ZnO. Further, Pt⁴⁺ was dispersed in the resulting polymer composites to obtain Pt NP-coated PPy-CB@ZnO NCs and was used as an electron-sensing substrate towards 4-NP in a phosphate buffer medium. Polypyrrole composites such as C-dots/PPy [19], PPy-CS-Fe₃O₄/ITO NCs [20], and PPy/C-doped ZnO NCs [21] have been used as potential sensing materials for picric acid, glucose, and hydroquinone, respectively. On the other hand, mesoporous Si/PPy NCs [22], Ag-rGO NSs [23], and FeOx/TiO₂@C NCs [24] have shown a higher sensitivity with wider detection ranges of 1×10^{-8} – 1×10^{-2} M, 2.0–150.0 mM, and 5.0–310.0 μM, respectively, in the detection of 4-NP. Therefore, the electrochemical recognition of 4-NP using a GCE with Pt NP-embedded PPy-CB/ZnO NCs was achieved to enhance its parameters, such as sensitivity, LDR, LOD, stability, response time, and reproducibility.

2. Materials and Method

2.1. Chemical Reagents

Here, zinc acetate, Pluronic-F127 copolymer, polypyrrole-incorporated carbon black (CB), poly(3,4-ethylenedioxythiophene) polystyrene sulfonate (PEDOT:PSS), hexachloroplatinic (IV) acid hydrate, monosodium phosphate, disodium phosphate, acetic acid, hydrochloric acid, and ethanol (C₂H₅OH) were purchased from Sigma-Aldrich (St. Louis, MI, USA). These chemicals were used without further treatment. In the first

stage, the sol–gel method was utilized for the preparation of semiconductor metal oxide (ZnO), as per previous published work [25]. Shortly, 1.6 g of Pluronic F127 was dissolved in 30.0 mL of ethyl-alcohol with constant stirring for an hour. In this solution, 2.4 g of zinc acetate, 2.3 mL of CH_3COOH , and 0.74 mL of HCl were added and stirred for 60 min to prepare a homogeneous mixture. The solution was then left for 2 days at room temperature for proper polymerization and gel formation. The prepared mixture was then placed in a humidity chamber for aging, and finally dried at 65 °C overnight. The as-synthesized nanomaterial was then annealed at 450.0 °C for 4 h (heating at 1 °C/min and cooling at 1.0 °C/min to finally obtain the semiconductor metal oxide).

In the next step, an ultra-sonication route was used for the synthesis of 10% PPy-CB@ZnO NCs. Usually, 2.0 g of the prepared ZnO and 0.2 g of PPy-CB were stirred in 100.0 mL of double-distilled water for 15 min, followed by ultra-sonication for 30 min. The obtained mixture was properly filtered and washed (4–5 times) with ethanol and distilled water, before drying in an oven (65.0 °C/24 h) to achieve 10% PPy-CB@ZnO. Here, Pt^{4+} ions were well-dispersed into PPy-CB@ZnO composites utilizing a photo-chemical reduction approach to design Pt NP-decorated PPy-CB@ZnO NCs. Briefly, a required concentration of an H_2PtCl_6 solution in water containing 1.0 wt % Pt was added to a 1.0 g solution of 10% PPy-CB@ZnO in 100.0 mL of water. The suspending solution was irradiated for 14 h with an Osram Hg lamp with an illumination intensity of 2.0 mW/cm. Afterwards, filtration, washing, and drying in an oven at 65.0 °C for 24 h was performed to obtain 1% Pt-NP-embedded 10% PPy-CB@ZnO, designated as Pt-NP-embedded PPy-CB@ZnO NCs throughout this research article.

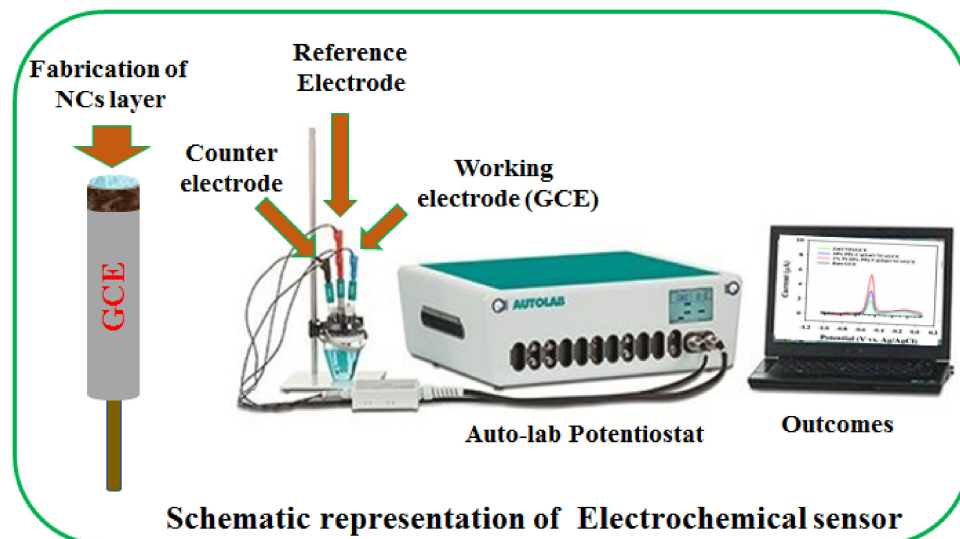
2.2. Materials Characterization

For the characterization of Pt-NPs-embedded PPy-CB@ZnO NCs, powder XRD investigations were conducted using a Bruker AXS-D4 Endeavour-X diffractometer (Radiation sources, $\text{CuK}\alpha_{1/2}$; $\lambda_{\alpha_1} = 154.060$ pm; $\lambda_{\alpha_2} = 154.439$ pm). Morphological and surface-associated characterizations were made using a field-emission secondary electron microscope (FE-SEM) (JEOL-6300F, 5.0 kV; Tokyo, Japan) and a high-resolution transmission electron microscope (HR-TEM) (JEOL JEM-2100F-UHR; Tokyo, Japan), respectively. These microscopes are operated at 200.0 kV with a built-in 1K-CCD camera (Tokyo, Japan) and a Gatan GIF 2001 energy filter (Tokyo, Japan). For functional group characterization, FTIR analysis of KBr pellets in dispersion mode was performed with a Perkin Elmer Raman Station 400 spectrometer (Waltham, MA, USA) (range from 400 to 4000 cm^{-1}). A VGESCALAB 200R spectrometer (Waltham, MA, USA) fitted with an $\text{MgK}\alpha$ ($h\nu = 1253.6$ eV) non-monochromatic X-ray source and a hemispherical electron analyzer was used to perform X-ray photoelectron spectroscopy (XPS) analysis. During the initial treatment process, freshly prepared samples were degassed, before they were shuffled in an ultra-high vacuum analysis chamber for 1 h. A Quantachrome NOVA 4200 analyzer (Florida, USA) was used at a temperature of 77.0 K to acquire the nitrogen adsorption isotherm for surface analysis. Each sample was degassed at 200.0 °C overnight. The nanocomposite surface area was measured via the Brunauer–Emmett–Teller (BET) technique using adsorption data. Diffuse reflectance spectra in a range from 200 to 800 nm were obtained on a UV–Vis spectrophotometer (Shimadzu: UV-3600 plus, Tokyo, Japan).

2.3. Fabrication of a GCE Using Pt NP-Embedded PPy-CB@ZnO NCs

Modification of GCE to a working electrode is a critical task in the sensor development. To do this, the prepared NCs were used to make slurry in ethanol, and they were used to coat the GCE surface in a way that yielded a uniform thin layer of NCs on the GCE (Surface area 0.0316 cm^2). 10.0 μL of PEDOT:PSS were added to serve as the polymer mixture on the GCE. After drying, the modified GCE, acting as a working electrode, was supplemented with Metrohm-Autolab modules (Malden, MA, USA) at a parallel connection with an Ag/AgCl column electrode and a Pt wire (used as reference) and counter electrodes, respectively. The target analyte (4-NP) was analyzed electrochemically at a concentration range of

1.5~40.5 μM . The obtained data (e.g., sensitivity, response time, LOD, LOQ, reproducibility, and LDR) were evaluated. Finally, the real samples contaminated with 4-NP were measured. Scheme 1 represents the sensor fabrication and settings with the potentiostat.



Scheme 1. Modification of GCE with Pt-NPs-decorated PPy-CB@ZnO NCs using PEDOT:PSS binder.

3. Results and Discussion

3.1. Morphological Analysis of Pt NP-Embedded PPy-CB@ZnO NCs

Figure 1 represents the FESEM analysis of the Pt NP-embedded PPy-CB@ZnO NCs. As presented in Figure 1a, the shape of the pure ZnO exhibits a capsule-like structure. When it was composited with polypyrrole (PPy) and carbon black (CB), the prepared ZnO particles were adsorbed onto the surface and formed a shape without any particular structure, as demonstrated in Figure 1b. After the addition of Pt nanoparticles by photo-reduction, they were also deposited onto the surface of the PPy-CB@ZnO NCs, resulting in a spherical shape. Thus, Pt NP-embedded PPy-CB@ZnO is considered a nanocomposite (NC). Analogous to Figure 1, a highly magnified EDS image exhibited nanocomposite-shape, as shown in Figure 2a. The elemental analysis obtained by EDS (selected area) confirms the existence of 25.07% C, 1.24% N, 16.51% O, 55.76% Zn, and 1.35% Pt, as presented in Figure 2b. Therefore, EDS analysis provides evidence of the existence of C, N, O, Zn, and Pt in the prepared Pt NPs-embedded PPy-CB@ZnO NCs.

For a detailed morphological analysis of Pt-NP-decorated PPy-CB@ZnO NCs, HRTEM was employed to confirm their structure. The obtained images are presented in Figure 3. Figure 3a shows the capsule structure of ZnO. Similarly, Figure 3b–d show the irregular adsorption of ZnO on the surface of PPy-CB and subsequently, Pt-NPs on PPy-CB@ZnO, respectively, not forming any particular shape. From the magnified HRTEM images, the lattice spacing (Figure 3e) was calculated as 0.27 nm, and the SAED is given in Figure 3f.

The active surface area was measured for the Pt-NP-embedded PPy-CB@ZnO NC materials and is presented in Figure 4. Here, the characteristics of the prepared NCs are clarified through a nitrogen adsorption/desorption isotherm, known as BET analysis. A plot of the relative pressure versus the adsorption of nitrogen gas was used to calculate the relative surface area of NCs found as 78.18 m^2/g . The surface area is significantly improved for the NCs (blue line; 78.18 m^2/g) compared to only ZnO (green line; 14.61 m^2/g) due to the increasing the functional active site by different components in the NCs. Therefore, the morphological studies of the NCs showed the surface area value is favorable to electro-catalytic performance of the fabricated sensor probe.

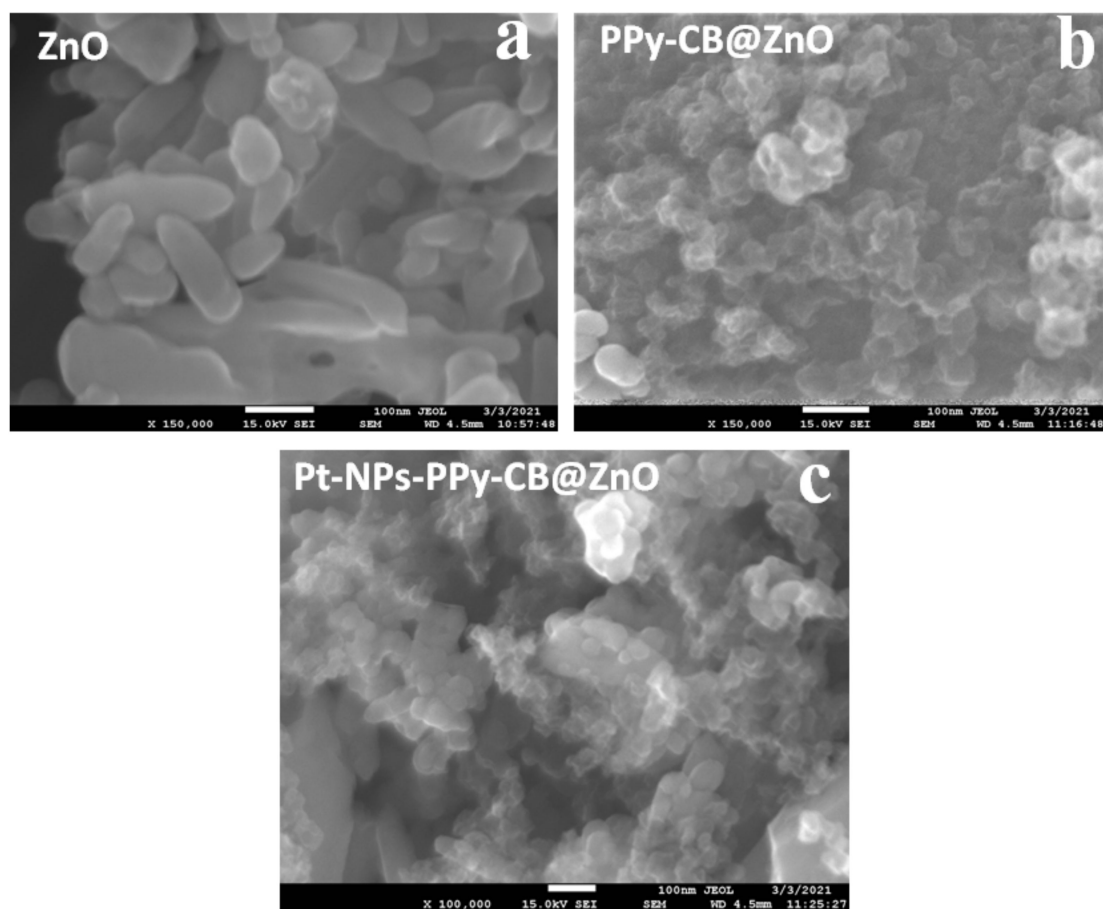


Figure 1. The FESEM analysis of Pt NPs-embedded PPy-CB@ZnO NCs explored (a) the capsule-like structure of ZnO, (b) the image of PPy-CB@ZnO, and (c) the nanocomposite structure of prepared Pt NPs-embedded PPy-CB@ZnO.

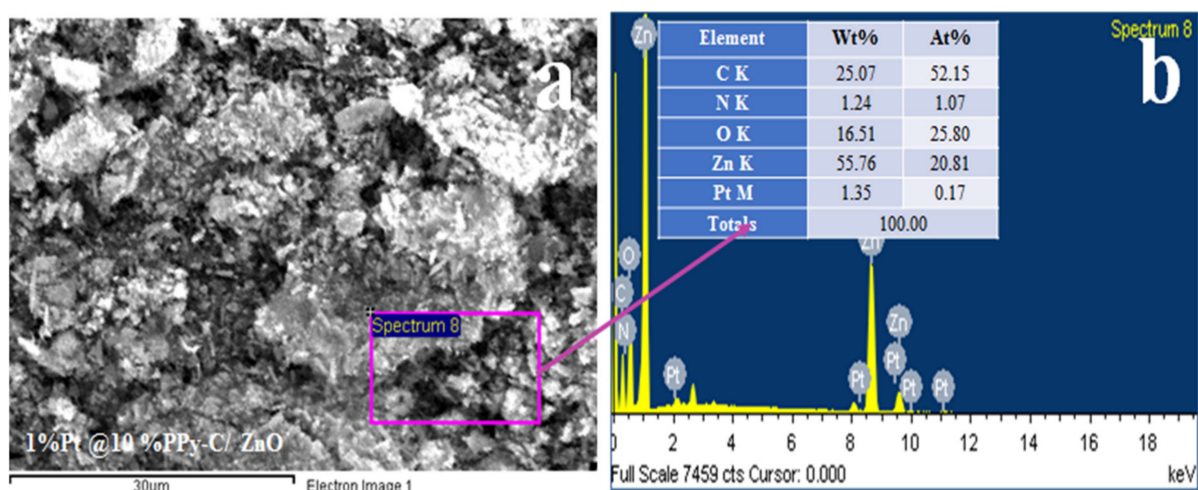


Figure 2. EDS analysis of Pt NPs- embedded PPy-CB@ZnO NCs; (a) Higher magnifying image of Pt-NPs PPy-CB@ZnO NCs and (b) Elemental composition spectrum of synthesized Pt NPs- embedded PPy-CB@ZnO NCs (Composition of elements; Inset; Table).

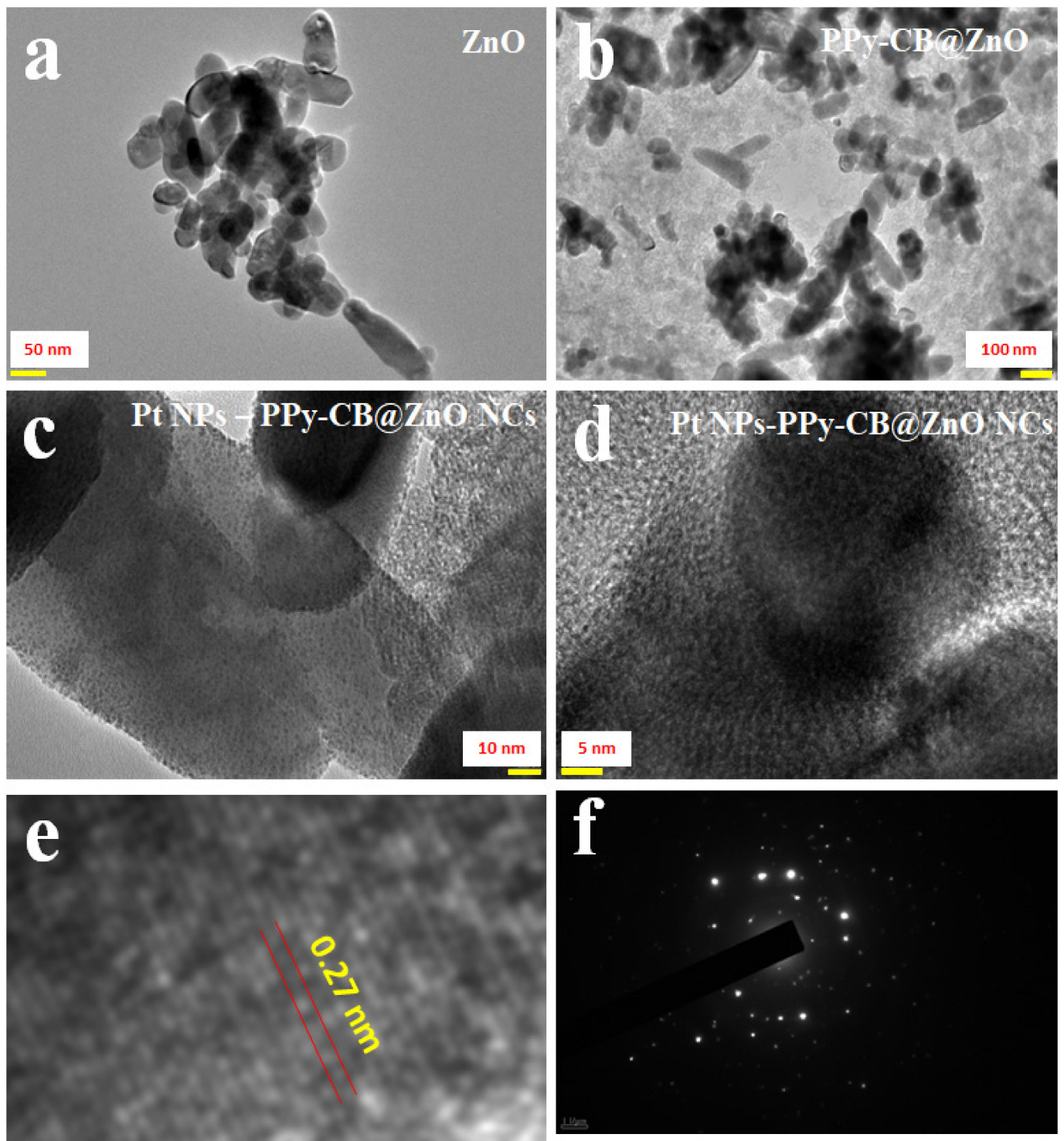


Figure 3. HRTEM analysis of Pt NPs-embedded PPy-CB@ZnO NCs; (a) ZnO, (b) PPy-CB@ZnO, (c,d) Low-to-high magnified Pt NPs-embedded PPy-CB@ZnO NCs, (e) Lattice spacing of NCs, and (f) diffraction pattern (SAED) of NCs.

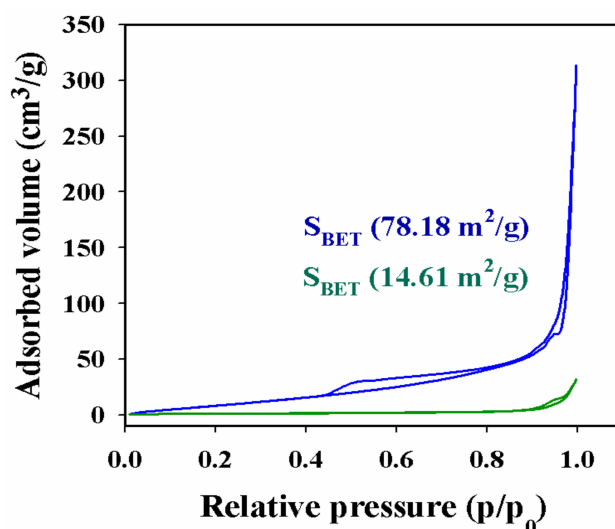


Figure 4. The BET analysis of Pt-NPs-embedded PPy-CB@ZnO NCs (blue line) and ZnO (green line).

3.2. Surface Composition by XPS Analysis

XPS analysis of the Pt-NP- embedded PPy-CB@ZnO NCs was performed to identify the oxidation states of the individual constituting atoms, as demonstrated in Figure 5. The survey spectrum of NCs has been analyzed by XPS, and it is presented in Figure 5a. The XPS spectrum of Pt4f_{7/2} and Pt4f_{5/2} is fitted with the binding energies of 75.5 and 78.5 eV, respectively, as shown in Figure 5b, which has been found for Pt⁴⁺ ionization, as reported elsewhere [26,27]. Nitrogen is a constituting element of Pt-NP-embedded PPy-CB@ZnO NCs, and the N1s orbital is explored in Figure 5c. As shown, the three bonds of nitrogen are positioned at 399, 401, and 402 eV, corresponding to N-H₂, N-H, and N-C, respectively [28,29]. O1s also shows three bonds, Zn-O, C-O, and C=O, placed at 530, 531, and 531.6 eV, respectively, and confirmed the oxygen (II) oxidation state illustrated in Figure 5d [30]. Carbon is another constituting element of NCs, and the C1s orbital is illustrated in Figure 5e and contains C-C, C-O, and O=C-O bonds, which are located at 283, 284.5, and 286 eV, in accordance with results reported elsewhere [31,32]. As displayed in Figure 5f, the Zn2p orbital exhibits two-spin orbitals Zn2p_{5/2} and Zn2p_{3/2}, positioned at 1022 and 1045 eV, respectively. The 23.0 eV energy difference between these two spin orbitals confirmed the existence of the Zn²⁺ oxidation state in the prepared NCs [33,34].

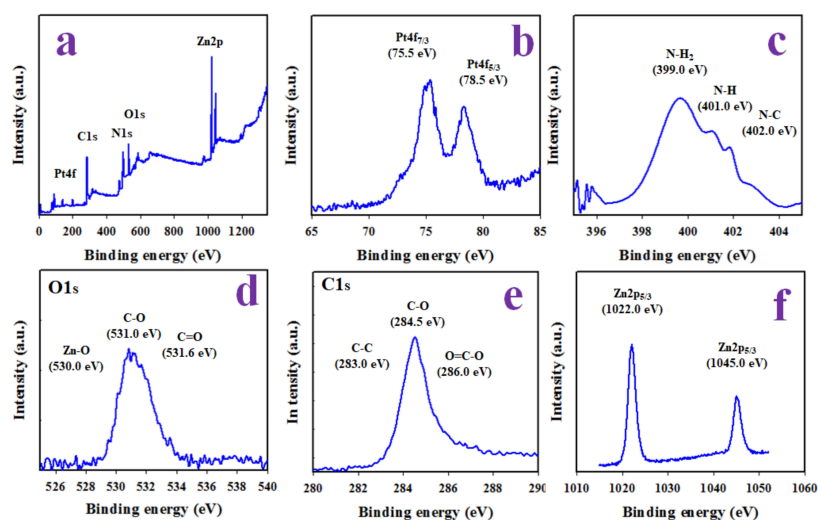


Figure 5. XPS analysis of Pt-NPs-embedded PPy-CB@ZnO NCs; (a) survey spectrum, (b) Pt4f, (c) N1s, (d) O1s, (e) C1s, and (f) Zn2p.

3.3. Structural and Optical Characterization of NCs

A crystallographic analysis of the synthesized NCs of the Pt-NP-embedded PPy-CB@ZnO NCs was performed, as illustrated in Figure 6a. The XRD pattern exhibits the crystalline planes of ZnO at (100), (002), (102), (110), (103), (112), and (201) only, also identified in previous reports [35,36]. The functional groups of the Pt-NP-embedded PPy-CB@ZnO NCs were subject to FTIR investigation, as illustrated in Figure 6b.

A peak was obtained at 500 cm^{-1} , identified as the stretching vibration of the Zn-O bond [37,38]. Using Tauc's equation, the optical band-gap energy of the NCs was calculated from the UV-visible absorbance, as presented in Figure 6c,d. As measured, the optical band-gap energy of the Pt-NP-embedded PPy-CB@ZnO NCs is equal to 2.8 eV, which is less than the bandgap of the PPy-CB@ZnO NCs (3.2 eV) and ZnO (3.0 eV). Therefore, the prepared Pt-NP-embedded PPy-CB@ZnO NCs have more conductivity compared to PPy-CB@ZnO and ZnO.

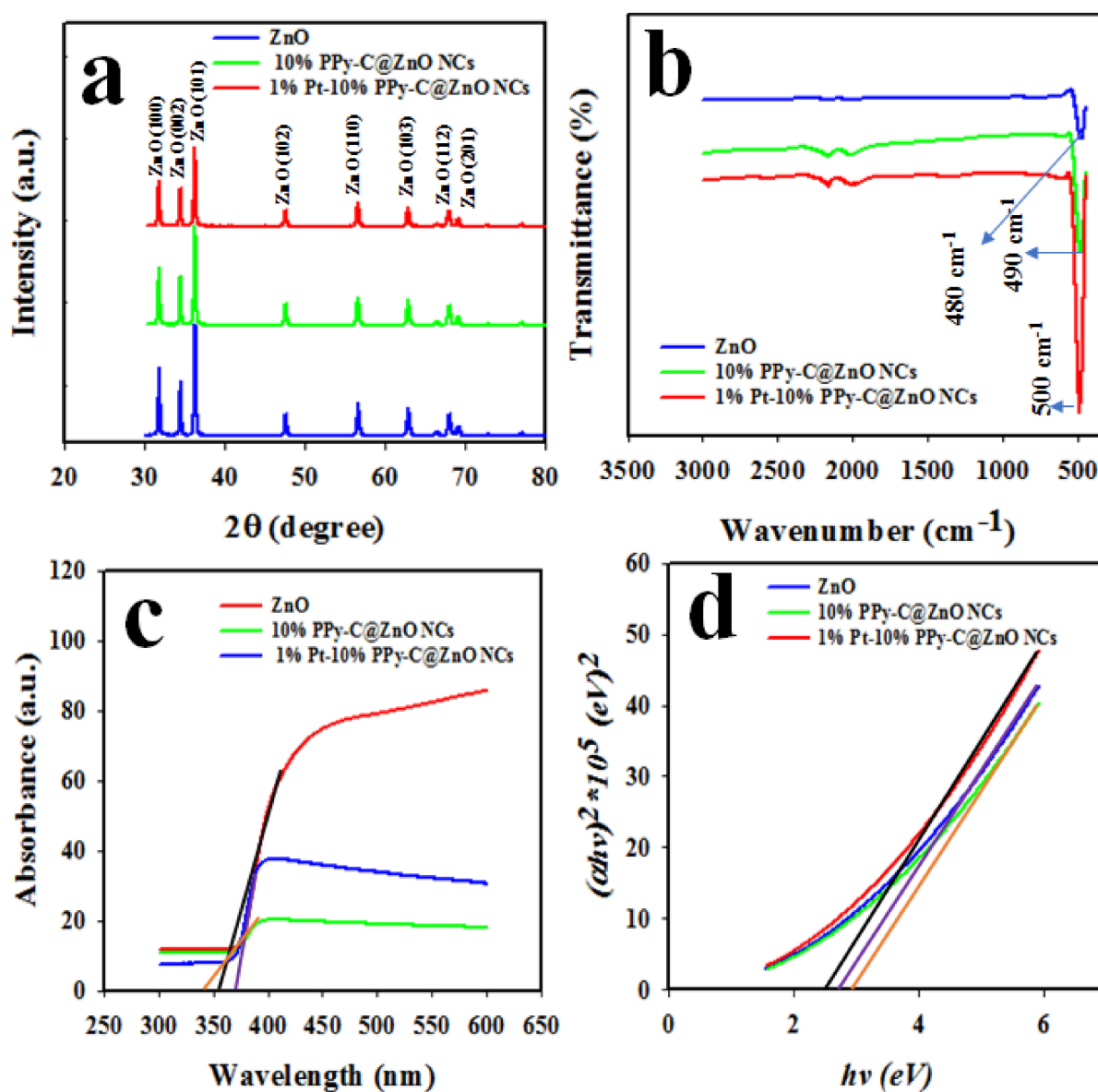


Figure 6. The structural and optical characterization of Pt-NP-embedded PPy-CB@ZnO NCs; (a) powder XRD pattern, (b) FTIR, (c) the UV-visible absorption by prepared NCs, and (d) Tauc's plot using the UV-visible optical absorbance.

3.4. Electrochemical Studies of Pt-NPs-Embedded PPy-CB@ZnO NCs

For the voltammetric characterization of the prepared Pt-NP-embedded PPy-CB@ZnO NCs/GCE, 0.1 mM $K_4[Fe(CN)_6]$ was used, as shown in Figure 7a. The separation potential between the oxidation and the reduction peak current of the coated GCE was +0.55 V. That of the bare GCE was +0.58 V, which is higher than that of the Pt-NP-embedded PPy-CB@ZnO NCs/GCE. Therefore, the working electrode based on the Pt-NP-embedded PPy-CB@ZnO NCs/GCE has more electric conductivity, favorable to the electrochemical analysis of an analyte. Similar observations have been described elsewhere [39,40]. Stability is an important sensor criterion in the electrochemical analysis of a working electrode. Thus, the stability of the Pt-NP-embedded PPy-CB@ZnO NCs/GCE was tested in the investigation of the 0.1 mM $K_4[Fe(CN)_6]$, as presented in Figure 7b, and 50 CV cycles were completely indistinguishable. It is evident in the analysis of $K_4[Fe(CN)_6]$ that the assembled working electrode has a high stability, and it can be assumed that other analytes will show a similar performance. To evaluate the molecular diffusion on the surface of the working electrode, a plot showing current versus the square root of the scan rate at a range of 25~300 mV/s is shown in Figure 7d. The experiment was conducted using 0.1 mM $K_4[Fe(CN)_6]$. The resulting peak currents are linearly distributed on the lines in both oxidation and reduction and can be expressed by the following equations (Equations (1) and (2)).

$$i_p = 85.265 (SR)^{1/2} + 222.8; R^2 = 0.9993 \text{ in oxidation of } K_4[Fe(CN)_6] \quad (1)$$

$$i_p = 57.885 (SR)^{1/2} - 173.17; R^2 = 0.9934 \text{ in reduction of } K_3[Fe(CN)_6] \quad (2)$$

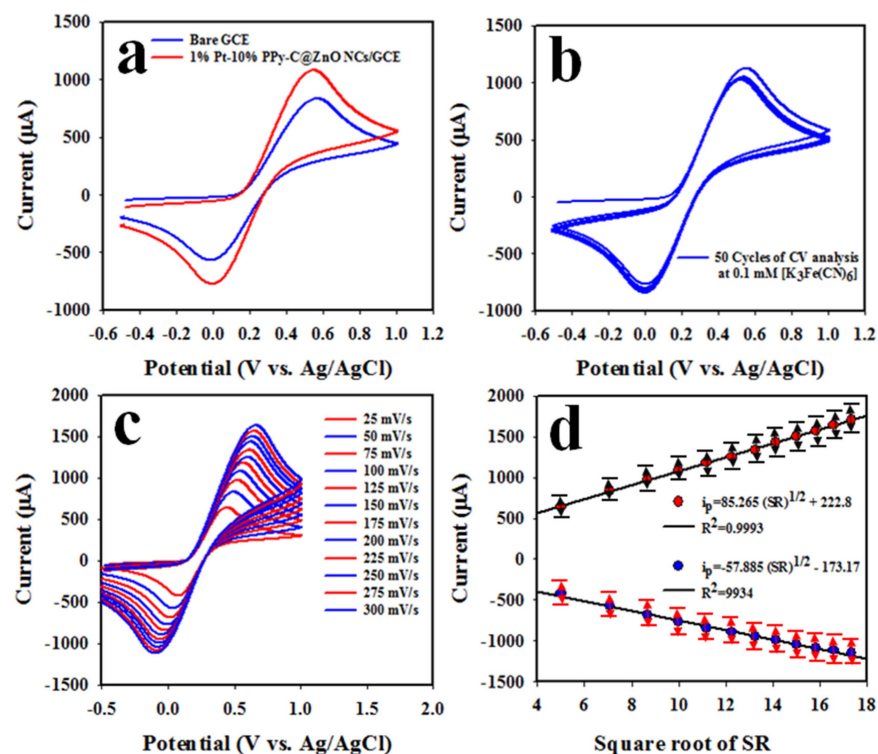


Figure 7. The electrochemical characterization of Pt-NPs- embedded PPy-CB@ZnO NCs/GCE by cyclic voltammetry; (a) The comparison of coated and bare-GCE in analysis of 0.1 mM $K_4[Fe(CN)_6]$, (b) stability of coated GCE, (c) scan rate at 25~300 mV/s, and (d) current versus square root of SR.

To justify the reactivity of Pt-NPs-embedded PPy-CB@ZnO NCs toward 4-NP, the constituting of each component of NCs were subjected to modify GCE individually and results are shown in Figure 8. As illustrated in Figure 8, Pt-NPs-embedded PPy-CB@ZnO

NCs/GCE has the highest electrochemical reactivity toward 4-NP in 16.5 μM concentration in a phosphate buffer medium of pH 7.0 compared to only bare GCE, PEDOT:PSS/GCE, ZnO/PEDOT:PSS/GCE, and PPy-CB@ZnO NCs/PEDOT:PSS/GCE electrodes. To execute this experiment, cyclic voltammetry has been applied in the detection of 4-NP in room conditions in presence of different modified electrodes. Peak current is increased significantly with the Pt-NPs-embedded PPy-CB@ZnO NCs electrode in identical conditions compared to other electrode assembly due to attachment of electro-active species (Pt-NPs) onto surface PPy-CB@ZnO NCs. In this case, the large surface area of synthesized Pt-NPs-embedded PPy-CB@ZnO NCs is involved as a substantial factor for this enhancement of resultant current and peak separation in electro-catalytic performance of nanomaterials.

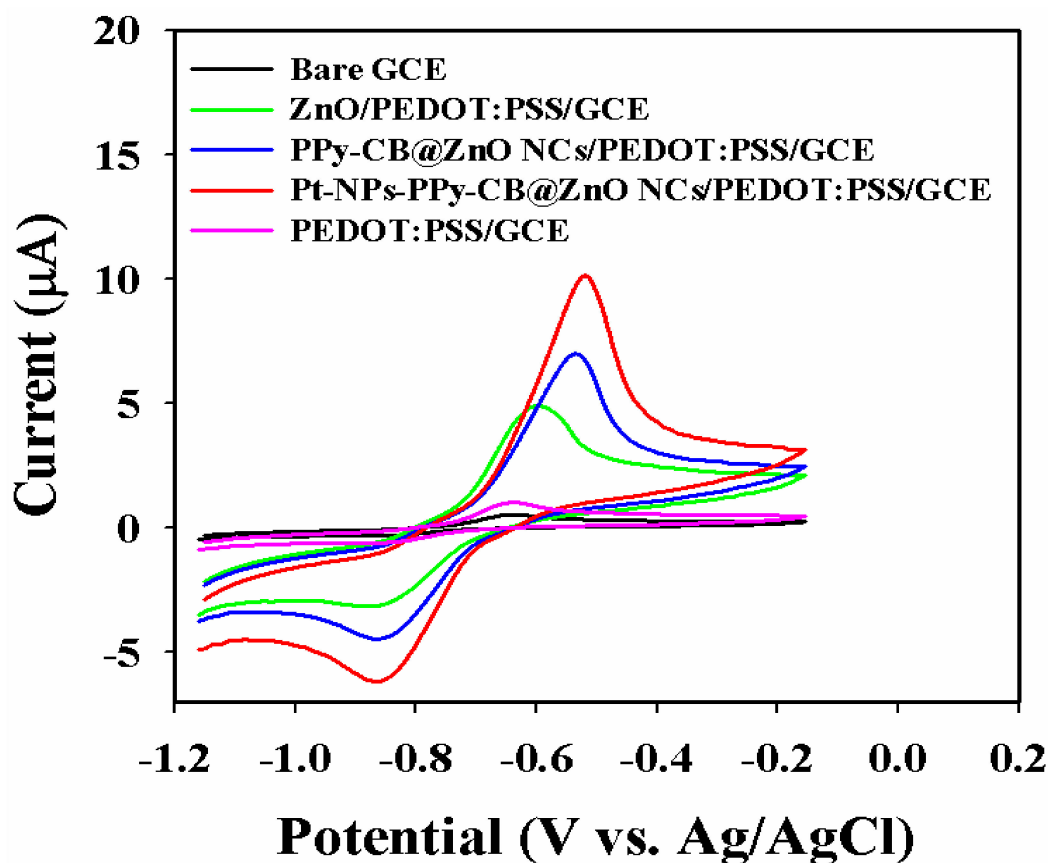


Figure 8. Control experiment executed at 16.5 μM of 4-NP using modified GCE with various nanomaterials of constituting elements of Pt-NPs-embedded PPy-CB@ZnO NCs.

The two equations above confirm good linearity and that the rate of reactions is diffusion-controlled rate of molecules on the working electrode surface, which has also been shown by previous authors [41]. In the current approach, differential pulse voltammetry (DPV) is a potential electrochemical method for analyzing an analyte. Therefore, 4-NP in a buffer medium of pH 7.0 was subject to DPV analysis based on a concentration range of 1.5–40.5 μM , as presented in Figure 9a. It is clear that the intensity of the peak current decreased (4-NP reduction held on -0.5 V) as the concentration of 4-NP increased. Thus, peak current points are plotted against the corresponding concentrations of 4-NP in Figure 9b.

The obtained current is distributed in a linear manner at a 4-NP concentration range of 1.5–40.5 μM , which was denoted as the detection range (LDR) of 4-NP for the assembled electrochemical sensor. Sensor parameters such as sensitivity ($7.8892 \mu\text{A}\mu\text{M}^{-1} \text{cm}^{-2}$) were calculated from the slope of the LDR ($0.2493 \mu\text{A}\mu\text{M}^{-1}$) by considering the apparent surface area of the GCE (0.0316cm^2). The LOD is estimated as $1.25 \pm 0.06 \mu\text{M}$, which is calculated

from $3 \times SD/\sigma$ (SD: Standard deviation of blank response; σ : Slope of the calibration curve). Limit of quantification (LOQ) is also calculated as $3.79 \mu\text{M}$ from $LOQ = 10LOD/3.3$. The linear equation of LDR can be expressed by Equation (3) as follows.

$$i_p = 0.2493 C(\mu\text{M}) + 15.694; R = 0.9917 \text{ in reduction of 4-NP} \quad (3)$$

A control experiment was performed, as illustrated in Figure 10a, to evaluate the reduction performances of 4-NP by the constituting elements of the prepared NCs, such as ZnO, PPy-CB@ZnO, and Pt-NPs on the PPy-CB@ZnO NC-coated GCE.

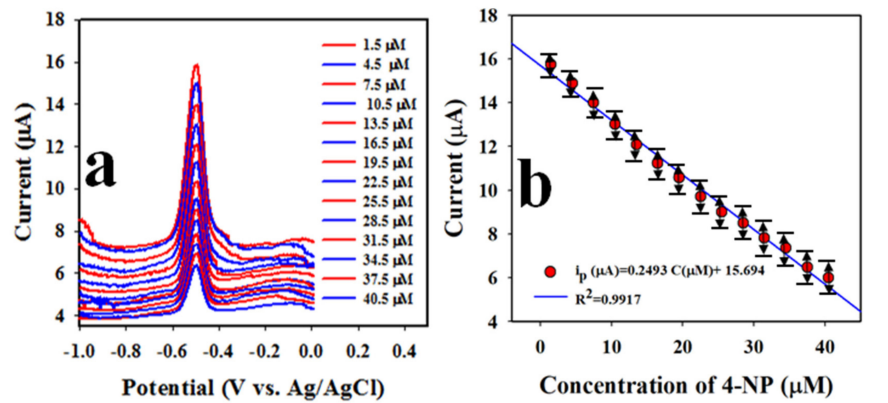


Figure 9. Detection of target analyte with Pt-NPs-embedded PPy-CB@ZnO NCs/GCE; (a) the resulted DPV analysis of 4-NP at 7.0 pH buffer and (b) calibration of 4-NP sensor obtained from current versus concentration of 4-NP.

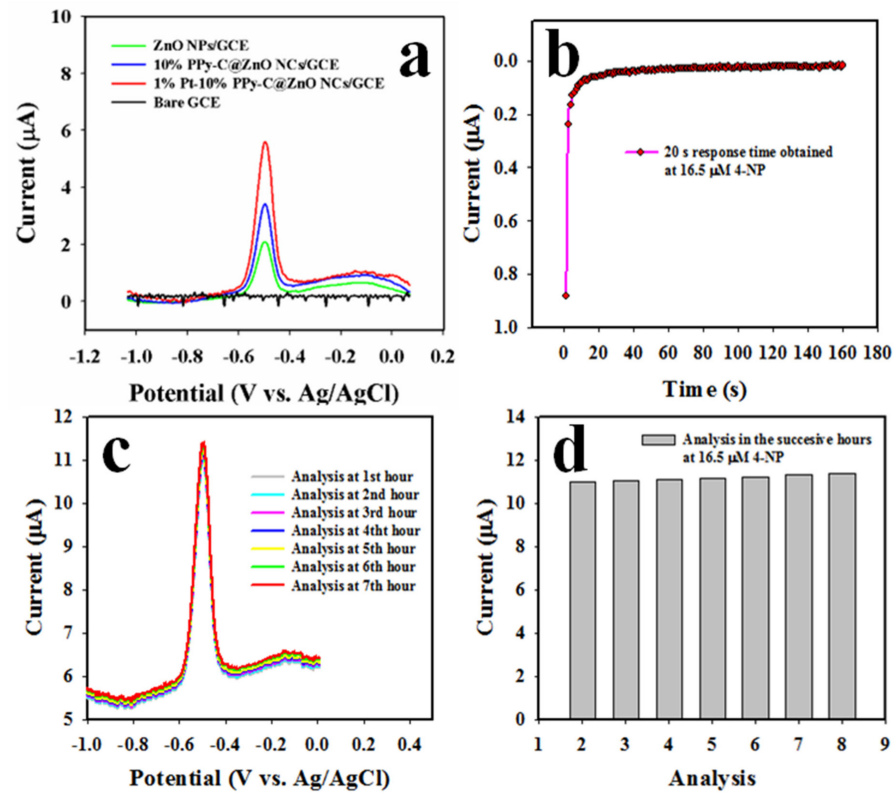


Figure 10. Analysis of sensor performance; (a) Control experiment in DPV analysis of 4-NP, (b) Response time at current versus time, (c) Reproducibility of 4-NP sensor, and (d) Reproducibility bar diagram.

The GCE modified by Pt-NPs-embedded PPy-CB@ZnO NCs has the highest peak current, and the bare GCE has a zero peak current. Thus, for 4-NP analysis, Pt-NPs-PPy-CB@ZnO NCs reasonably improved the conductivity of the working electrode via the DPV method. To specify the response of the 4-NP sensor, 16.5 μM of 4-NP was subjected to analysis, and the results are plotted as current versus time in Figure 10b. The current responses became steady at 20 s. Thus, 20 s was considered the response time of the 4-NP sensor for electrochemical analysis. The reproducibility of an electrochemical sensor is an important parameter that provides reliability information about it. Thus, the reproducibility test was executed by reaping seven analyses of 4-NP at 16.5 μM in a phosphate buffer medium of pH 7.0 using the sample working electrode, as shown in Figure 10c and a bare diagram in Figure 10d. As shown, the currents at the peak point in the reduction of 4-NP are changed and cannot be separated from each other. The related standard deviation was calculated and found as 1.28%. Thus, this test confirms that the assembled sensor based on the Pt-NPs-embedded PPy-CB@ZnO NCs/GCE has good reliability for analyzing 4-NP.

The pH value of the buffer medium is an influencing parameter to analyze the toxic chemical. Therefore, a number of buffer media with various pH values ranging from acidic to basic (pH 5.0 to pH 9.0) was subjected to analyze the response of 4-NP and are presented in the Figure 11a. As illustrated, the 4-NP sensor with Pt-NPs-embedded PPy-CB@ZnO NCs-sensing substrate shows the highest current at pH 7.0 compared to other pH values. Thus, pH 7.0 of phosphate buffer medium is optimized and used for measuring by the DPV analysis to detect 4-NP with Pt-NPs-embedded PPy-CB@ZnO NCs/GCE electrode in room conditions. Selectivity is another significant parameter of any newly fabricated sensor probe to show in which chemical it is more efficient in detecting the target analyte. Therefore, a number of toxic chemicals including chlorobenzene (CB), phenyl-hydrazine (Phyd), 3-chlorophenol (3-CP), 1,2-diaminobenzene (1,2-DAB), 4-aminophenol (4-AP), and 4-nitrophenol (4-NP) were taken to DPV analysis with GCE-modified Pt-NPs-embedded PPy-CB@ZnO NCs. The results are presented in Figure 11b. As shown, for 4-NP it exhibited the highest peak current (magnitude) compared to other chemicals in similar measurements in identical conditions. Other chemicals are not found to have any enhanced current response towards the sensing substrate (Pt-NPs- embedded PPy-CB@ZnO NCs) in 7.0 pH buffer medium. It can be concluded that Pt-NPs-embedded PPy-CB@ZnO NCs/GCE electrode has detected selectivity of 4-NP, only compared to other interferences.

To realize the stability of Pt-NPs embedded PPy-CB@ZnO NCs/GCE sensor probe, the repeatability performance was tested again but for elongated period around seven consecutive days, as illustrated in Figure 11c. A similar observation is perceived as in the Figure 10c. This experiment was performed at 4.5 μM of 4-NP in a buffer medium of pH 7.0. Thus, it can be predicted that the 4-NP sensor based on Pt-NPs-embedded PPy-CB@ZnO NCs/GCE is stable in its performance. To investigate the interference of 4-NP sensor probe, the 4-NP was analyzed by DPV in presence of CB, 4-AP, 1,2-DAB and CB, as illustrated in Figure 11d. It is perceived that the 4-NP sensor probe has not any measurable interference in presence of other toxic chemicals.

Comparison studies of 4-NP sensors based on various sensing electrode materials are demonstrated [42–51] in Table 1.

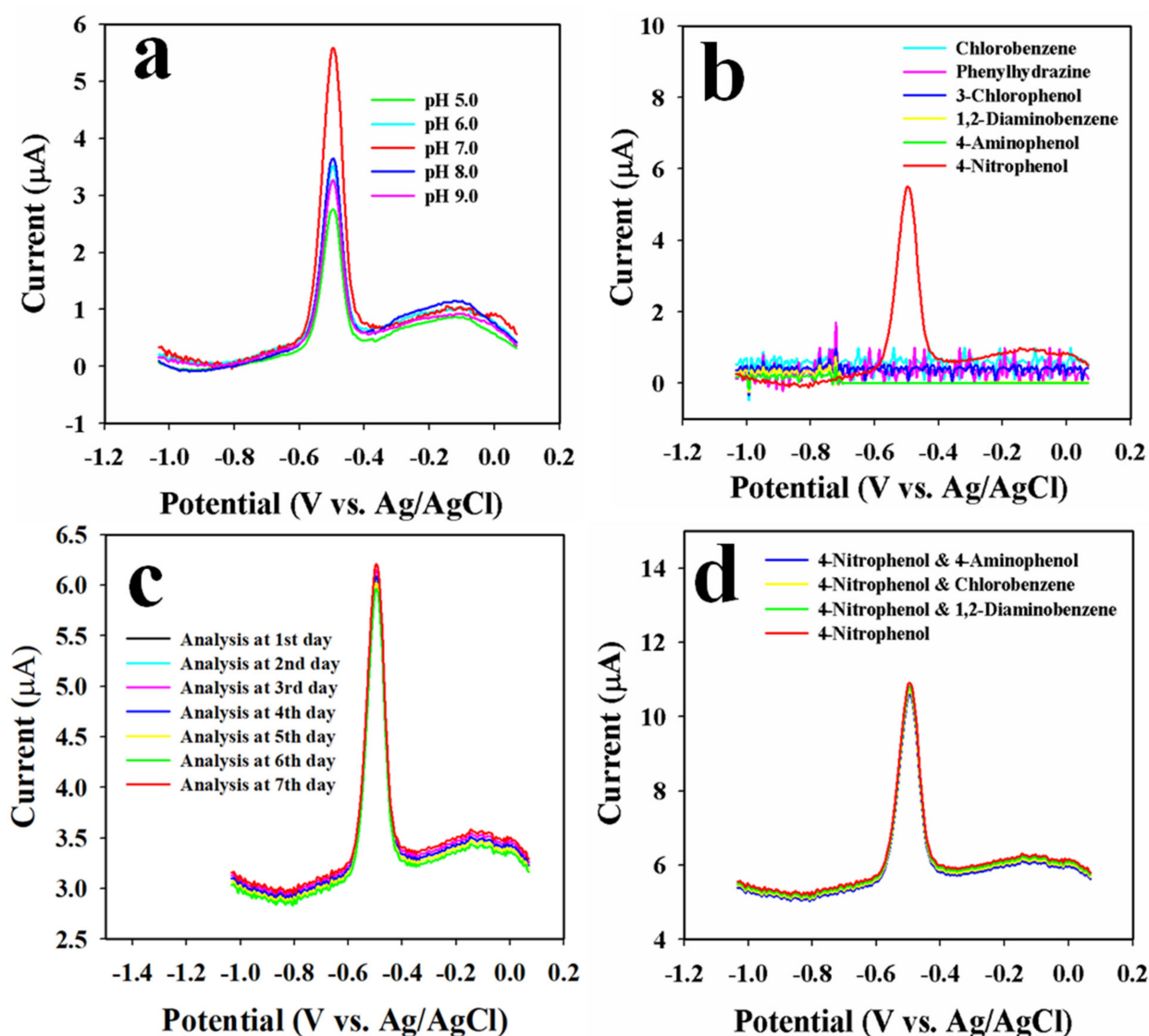
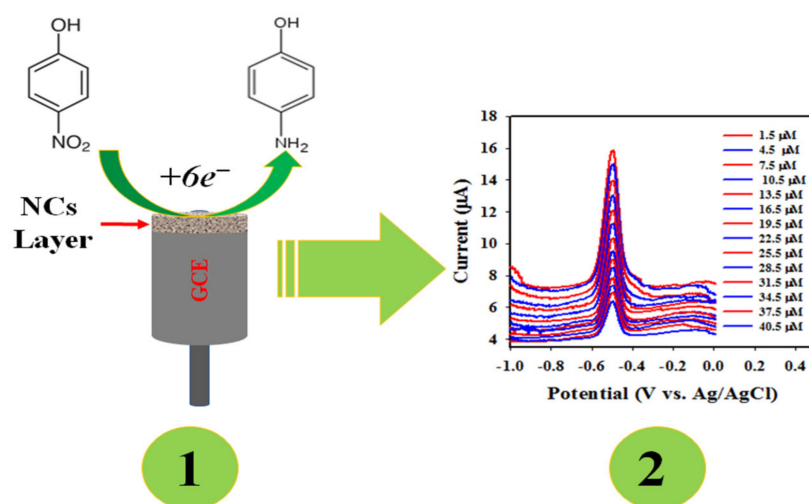
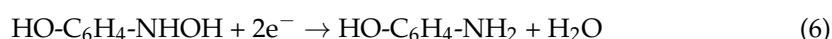


Figure 11. (a) The DPV investigation of 4-NP analysis at distinct pH value of buffer medium, (b) DPV analysis of various toxic chemicals in 16.5 μM concentration, (c) the repeatability performance of 4-NP sensor at 4.5 μM concentration of 4-NP I buffer medium of pH 7.0, and (d) interference effects of 4-NP sensor probe.

Table 1. Comparison of sensor performances with various modified electrode towards the detection of 4-NP by an electrochemical approach.

| Electrode Materials | LOD | LDR | Sensitivity | Ref. |
|--|----------------------|--|--|------------|
| PCZ/N-GE/GCE | 0.062 μM | $8 \times 10^{-7} \sim 2 \times 10^{-5} \text{ M}$ | — | [42] |
| S-GCN NSs | 0.0016 μM | 0.05~90 μM | — | [43] |
| NiO/CeO ₂ NCs/GCE | 2.48 μM | 1~20 μM | 3.68 $\mu\text{A}\mu\text{M}^{-1} \text{ cm}^{-2}$ | [44] |
| BaSnO ₃ -gC ₃ N ₄ NCs/GCE | 1.0 μM | 1.6~50 μM | 0.81 $\mu\text{A}\mu\text{M}^{-1} \text{ cm}^{-2}$ | [45] |
| Au-NP/RGO NCs/GCE | 0.01 μM | 0.05~2.0 μM | — | [46] |
| Au/CaCO ₃ NCs | 0.54 nM | 0.1~100 μM | — | [47] |
| PDDA-G NCs/GCE | 0.02 μM | 0.06~110 μM | — | [48] |
| RGO-MIP NCs | 0.005 μM | 0.01~100.0 μM | — | [49] |
| GO/GCE | 0.02 μM | 0.1~120 μM | — | [50] |
| Ag-NWs-PANI NCs/GCE | 52.0 nM | 0.6~32 μM | — | [51] |
| Pt NPs-PPy-CB@ZnO NCs/GCE | 12.50 nM | 1.5~40.5 μM | 7.89 $\mu\text{A}\mu\text{M}^{-1} \text{ cm}^{-2}$ | This study |

As shown in Table 1, the 4-NP sensor based on the PEDOT:PSS/GCE modified by Pt NPs-embedded PPy-CB@ZnO NCs exhibited improved performances in terms of sensitivity, LOD, and LDR. The electrochemical quantification of 4-NP based on Pt NPs-embedded PPy-CB@ZnO NCs/GCE is presented in Scheme 2. As shown, 4-NP is adsorbed on the surface of the modified GCE. Due to the applied potential, it is reduced to 4-aminophenol, as indicated in the reaction scheme below. Comparable electrochemical reduction reactions of 4-NP are reported in other articles [52–54]. The suggested electrochemical reduction reaction of 4-NP on the Pt NPs-embedded PPy-CB@ZnO NCs/GCE surface is as follows (Equations (4)–(6)):



Scheme 2. Schematic representation of chemical sensing; (1) electrochemical reduction of 4-NP and (2) the concentration-based responses of 4-NP to 4-AP.

Finally, the Pt-NP-embedded PPy-CB@ZnO NCs/PEDOT:PSS/GCE-fabricated sensor probe was used for the sensor validation by electrochemical analysis with real environmental samples, which were collected from various environmental sources, including underground water, tap water, and sea water. This also facilitated validation of the feasibility of 4-NP in environmental collected water samples. No electrochemical response of 4-NP was found in all the samples, which may be due to the absence of 4-NP in the water samples or because the concentration of 4-NP was lower than the method's detection limit. Therefore, this validity analysis was performed by applying the recovery standard addition method in room conditions. For validity, the real water substrates are spiked with 4-NP. The spiked concentration of 4-NP was measured based on the calibration curve, which is shown in Figure 9b. The data of real sample analyses are presented in Table 2. The 4-NP sensor based on the Pt-NP-embedded PPy-CB@ZnO NCs/PEDOT:PSS/GCE is shown to be reliable, with acceptable results [55–64]. Thus, the sensor can potentially be used for the development of micro-sized electrochemical devices by using an electrochemical approach.

Table 2. Validity analysis of environmental real-samples with Pt-NPs-embedded PPy-CB@ZnO NCs/PEDOT:PSS/GCE sensor probe, using an electrochemical approach.

| Real Samples | Added 4-NP Conc. (μM) | Found 4-NP Conc. ^a (μM) | | | Average Recovery ^b (%) | RSD ^c (%) ($n = 3$) |
|-------------------|------------------------------------|---|-------|-------|-----------------------------------|----------------------------------|
| | | R1 | R2 | R3 | | |
| Underground water | 16.50 | 16.46 | 16.37 | 16.42 | 99.49 | 0.27 |
| | 7.20 | 7.05 | 7.08 | 6.89 | 97.31 | 0.34 |
| Sea water | 16.50 | 16.27 | 16.35 | 16.47 | 99.17 | 0.62 |
| | 7.20 | 6.92 | 7.04 | 6.99 | 96.99 | 0.39 |
| Tap water | 16.50 | 16.21 | 16.15 | 16.19 | 98.08 | 0.19 |
| | 7.20 | 7.03 | 7.08 | 6.97 | 96.30 | 0.36 |

^a Mean of three repeated determination with Pt-NP-embedded PPy-C@ZnO NCs/PEDOT:PSS/GCE. ^b Concentration of 4-NP determined/Concentration taken. (Unit: μM). ^c Relative standard deviation value indicates precision among three repeated measurements (R1, R2, & R3).

4. Conclusions

In this approach, the Sol-gel prepared nanocomposites (NCs) of Pt-NP-embedded polypyrrol carbon black-embedded ZnO (PPy-CB@ZnO) show a highly significant structural morphology, which is favorable to the electrochemical detection of 4-NP in a phosphate buffer medium at pH 7.0. A working electrode was fabricated with the help of a conducting coating binder (PEDOT:PSS) to stick the NCs onto the surface of the sensor probe. The fabricated sensor probe based on the Pt-NP-embedded PPy-CB@ZnO NCs/PEDOT:PSS/GCE was used for the detection of 4-NP in a wider range of 1.5~40.5 μM by using PEDOT:PSS. Besides this, the fabricated sensor probe exhibited the highest sensitivity ($7.8892 \mu\text{A}\mu\text{M}^{-1} \text{cm}^{-2}$) and a relatively low LOD ($1.25 \pm 0.06 \mu\text{M}$) and LOQ (3.79 μM). In addition, it has good reproducibility as well as a short response time. The 4-NP sensor was applied to analyze a real sample and exhibited significant and reliable performance. Thus, it introduced an easy-to-use approach in using an electrochemical technique for developing a nanocomposite-based sensor probe, and it has potential environmental applications for the safety of environmental fields on a broad scale.

Author Contributions: Conceptualization, M.F. and M.M.R.; methodology, M.F. and M.M.A.; validation, M.M.A., M.M.R. and A.M.A.; formal analysis, M.F., M.M.A. and M.J.; investigation, M.F. and M.M.R.; resources, A.M.A., M.J. and F.A.H.; data curation, J.A., M.J. and R.S.A.; writing—original draft preparation, M.M.A. and M.M.R.; writing—review and editing, M.F., F.A.H., J.A., M.J., R.S.A. and A.M.A.; supervision, F.A.H. and A.M.A.; project administration, M.F. and F.A.H.; funding acquisition, M.F. and F.A.H. All authors have read and agreed to the published version of the manuscript.

Funding: This research was funded by the grant code (NU/RG/SERC/11/18) from the Deanship of Scientific Research at Najran University, Saudi Arabia.

Institutional Review Board Statement: Not applicable.

Informed Consent Statement: Not applicable.

Data Availability Statement: Data will be available upon reasonable request.

Acknowledgments: The authors are thankful to the Deanship of Scientific Research at Najran University for funding this work under the Research Groups Funding Program grant code (NU/RG/SERC/11/18).

Conflicts of Interest: The authors declare no conflict of interest.

References

- Serrà, A.; Artal, R.; Pozo, M.; Garcia-Amorós, J.; Gómez, E. Simple Environmentally-Friendly Reduction of 4-Nitrophenol. *Catalysts* **2020**, *10*, 458. [[CrossRef](#)]
- Chang, Y.C.; Chen, D.H. Catalytic reduction of 4-nitrophenol by magnetically recoverable Au nanocatalyst. *J. Hazard. Mater.* **2009**, *165*, 664–669. [[CrossRef](#)] [[PubMed](#)]

3. Rahman, M.M.; Wahid, A.; Alam, M.M.; Asiri, A.M. Efficient 4-Nitrophenol sensor development based on facile Ag@Nd₂O₃ nanoparticles. *Mater. Today Commun.* **2018**, *16*, 307–313. [[CrossRef](#)]
4. Abaker, M.; Dar, G.N.; Umar, A.; Zaidi, S.A.; Ibrahim, A.A.; Baskoutas, S.; Al-Hajry, A. CuO Nanocubes Based Highly-Sensitive 4-Nitrophenol Chemical Sensor. *Sci. Adv. Mater.* **2012**, *4*, 893–900. [[CrossRef](#)]
5. Dunier, M.; Siwicki, A.K. Effects of pesticides and other organic pollutants in the aquatic environment on immunity of fish: A review. *Fish Shellfish Immunol.* **1993**, *3*, 423–438. [[CrossRef](#)]
6. Hwa, K.Y.; Sharma, T.S.K.; Ganguly, A. Design strategy of rGO–HNT–AgNPs based hybrid nanocomposite with enhanced performance for electrochemical detection of 4-nitrophenol. *Inorg. Chem. Front.* **2020**, *7*, 1981–1994. [[CrossRef](#)]
7. Nehru, R.; Gopi, P.K.; Chen, S.M. Enhanced sensing of hazardous 4-nitrophenol by a graphene oxide–TiO₂ composite: Environmental pollutant monitoring applications. *New J. Chem.* **2020**, *44*, 4590–4603. [[CrossRef](#)]
8. Antohe, I.; Iordache, I.; Antohe, V.A.; Socol, G. A polyaniline/platinum coated fiber optic surface plasmon-resonance sensor for picomolar detection of 4-nitrophenol. *Sci. Rep.* **2021**, *11*, 10086. [[CrossRef](#)]
9. Lupu, S.; Lete, C.; Marin, M.; Totir, N.; Balaure, P.C. Electrochemical sensors based on platinum electrodes modified with hybrid inorganic–organic coatings for determination of 4-nitrophenol and dopamine. *Electrochim. Acta* **2009**, *54*, 1932–1938. [[CrossRef](#)]
10. Ghazizadeh, A.J.; Afkhami, A.; Bagheri, H. Voltammetric determination of 4-nitrophenol using a glassy carbon electrode modified with a gold–ZnO–SiO₂ nanostructure. *Microchim. Acta* **2018**, *185*, 296. [[CrossRef](#)]
11. Nehru, R.; Chen, T.W.; Chen, S.M.; Tseng, T.W.; Liu, X. 4-nitrophenol Detection in Water Sample Using Linear Sweep Voltammetry with f-Multi Walled Carbon Nanotubes modified electrode. *Int. J. Electrochem. Sci.* **2018**, *13*, 7778–7788. [[CrossRef](#)]
12. Subhan, M.A.; Jhuma, S.S.; Saha, P.C.; Alam, M.M.; Asiri, A.M.; Al-Mamun, M.; Attia, S.A.; Emon, T.H.; Azad, A.K.; Rahman, M.M. Efficient selective 4-aminophenol sensing and antibacterial activity of ternary Ag₂O₃SnO₂Cr₂O₃ nanoparticles. *New J. Chem.* **2019**, *43*, 10352–10365. [[CrossRef](#)]
13. Yin, H.; Zhou, Y.; Ai, S.; Ma, Q.; Zhu, L.; Lu, L. Electrochemical oxidation determination and voltammetric behaviour of 4-nitrophenol based on Cu₂O nanoparticles modified glassy carbon electrode. *J. Environ. Anal. Chem.* **2012**, *92*, 742–754. [[CrossRef](#)]
14. Padmanaban, A.; Dhanasekaran, T.; Manigandan, R.; Kumar, S.P.; Gnanamoorthy, G.; Stephen, A.; Narayanan, V. Facile solvothermal decomposition synthesis of single phase ZnBi₃₈O₆₀ nanobundles for sensitive detection of 4-nitrophenol. *New J. Chem.* **2017**, *41*, 7020–7027. [[CrossRef](#)]
15. Wahid, A.; Asiri, A.M.; Rahman, M.M. One-step facile synthesis of Nd₂O₃/ZnO nanorods for an efficient selective 2,4-dinitrophenol sensor probe. *Appl. Surface Sci.* **2019**, *487*, 1253–1261. [[CrossRef](#)]
16. Zhou, W.S.; Zhao, B.; Huang, X.H.; Yang, X.D. Electrochemical Determination of 4-Nonylphenol on Graphene-Chitosan Modified Glassy Carbon Electrode. *Chinese J. Anal. Chem.* **2013**, *41*, 675–680. [[CrossRef](#)]
17. De-Lima, C.A.; da-Silva, P.S.; Spinelli, A. Chitosan-stabilized silver nanoparticles for voltammetric detection of nitrocompounds. *Sens. Actuators B Chem.* **2014**, *196*, 39–45. [[CrossRef](#)]
18. Giribabu, K.; Haldorai, Y.; Rethinasabapathy, M.; Jang, S.C.; Suresh, R.; Cho, W.S.; Han, Y.K.; Roh, C.; Huh, Y.S.; Narayanan, V. Glassy carbon electrode modified with poly(methyl orange) as an electrochemical platform for the determination of 4-nitrophenol at nanomolar levels. *Curr. Appl. Phys.* **2017**, *17*, 1114–1119. [[CrossRef](#)]
19. Pal, A.; Sk, M.P.; Chattopadhyay, A. Conducting Carbon Dot–Polypyrrole Nanocomposite for Sensitive Detection of Picric acid. *ACS Appl. Mater. Interfaces* **2016**, *8*, 5758–5762. [[CrossRef](#)]
20. AL-Mokaram, A.M.A.A.; Yahya, R.; Abdi, M.M.; Mahmud, H.N.M.E. One-step electrochemical deposition of Polypyrrole–Chitosan–Iron oxide nanocomposite films for non-enzymatic glucose biosensor. *Mater. Lett.* **2016**, *183*, 90–93. [[CrossRef](#)]
21. Ahmed, J.; Faisal, M.; Jalalah, M.; Alsareii, S.A.; Harraz, F.A. Novel polypyrrole-carbon black doped ZnO nanocomposite for efficient amperometric detection of hydroquinone. *J. Electroanal. Chem.* **2021**, *898*, 115631. [[CrossRef](#)]
22. Tighilt, F.Z.; Belhousse, S.; Rahal, A.; Hamdani, K.; Belhaneche, N.; Sam, S.; Lasmi, K. Mesoporous Silicon/Polypyrrole Based Structures for Paranitrophenol Sensing. *Silicon* **2022**, *14*, 4149–4155. [[CrossRef](#)]
23. Ahmad, N.; Al-Fatesh, A.S.; Wahab, R.; Alam, M.; Fakeeha, A.H. Synthesis of silver nanoparticles decorated on reduced graphene oxide nanosheets and their electrochemical sensing towards hazardous 4-nitrophenol. *J. Mater. Sci. Mater. Electron.* **2020**, *31*, 11927–11937. [[CrossRef](#)]
24. Wang, M.; Liu, Y.; Yang, L.; Tian, K.; He, L.; Zhang, Z.; Ji, Q.; Song, Y.; Fang, S. Bimetallic metal–organic framework derived FeOx/TiO₂ embedded in mesoporous carbon nanocomposite for the sensitive electrochemical detection of 4-nitrophenol. *Sens. Actuators B Chem.* **2019**, *281*, 1063–1072. [[CrossRef](#)]
25. Faisal, M.; Rashed, M.A.; Ahmed, J.; Alsaiani, M.; Alkorbi, A.S.; Jalalah, M.; Alsareii, S.A.; Harraz, F.A. Rapid photodegradation of linezolid antibiotic and methylene blue dye over Pt nanoparticles/polypyrrole-carbon black/ZnO novel visible light photocatalyst. *J. Environ. Chem. Eng.* **2021**, *9*, 106773. [[CrossRef](#)]
26. Hagiwara, H.; Nagatomo, M.; Seto, C.; Ida, S.; Ishihara, T. Dye Modification Effects on TaON for Photocatalytic Hydrogen Production from Water. *Catalysts* **2013**, *3*, 614–624. [[CrossRef](#)]
27. Wang, K.; Wang, H.; Pasupathi, S.; Linkov, V.; Ji, S.; Wang, R. Palygorskite promoted PtSn/carbon catalysts and their intrinsic catalytic activity for ethanol oxidation. *Electrochim. Acta* **2021**, *70*, 394–401. [[CrossRef](#)]
28. Majumdar, A.; Das, S.C.; Shripathi, T.; Hippler, R. Chemical synthesis and surface morphology of amorphous hydrogenated carbon nitride film deposited by N₂/CH₄ dielectric barrier discharge plasma. *Compos. Interfaces* **2012**, *19*, 161–170. [[CrossRef](#)]

29. Ravi, S.; Zhang, S.; Lee, Y.R.; Kang, K.K.; Kim, J.M.; Ahn, J.W.; Ahn, W.S. EDTA-functionalized KCC-1 and KIT-6 mesoporous silicas for Nd³⁺ ion recovery from aqueous solutions. *J. Ind. Eng. Chem.* **2018**, *67*, 210–218. [[CrossRef](#)]
30. Sadri, R.; Hosseini, M.; Kazi, S.N.; Bagheri, S.; Zubir, N.; Solangi, K.H.; Zaharinie, T.; Badarudin, A. A bio-based, facile approach for the preparation of covalently functionalized carbon nanotubes aqueous suspensions and their potential as heat transfer fluids. *J. Colloid. Interface Sci.* **2017**, *504*, 115–123. [[CrossRef](#)]
31. Xiao, S.; Xu, P.; Peng, Q.; Chen, J.; Huang, J.; Wang, F.; Noor, N. Layer-by-Layer Assembly of Polyelectrolyte Multilayer onto PET Fabric for Highly Tunable Dyeing with Water Soluble Dyestuffs. *Polymers* **2017**, *9*, 735. [[CrossRef](#)]
32. Bourlier, Y.; Bouttemy, M.; Patard, O.; Gamarra, P.; Piotrowicz, S.; Vigneron, J.; Aubry, R.; Delage, S.; Etcheberry, A. Investigation of InAlN Layers Surface Reactivity after Thermal Annealings: A Complete XPS Study for HEMT. *ECS J. Solid State Sci. Technol.* **2018**, *7*, P329–P338. [[CrossRef](#)]
33. Liang, Y.C.; Wang, C.C. Surface crystal feature-dependent photoactivity of ZnO–ZnS composite rods via hydrothermal sulfidation. *RSC Adv.* **2018**, *8*, 5063–5070. [[CrossRef](#)]
34. Xu, D.; Fan, D.; Shen, W. Catalyst-free direct vapor-phase growth of Zn_{1-x}Cu_xO micro-cross structures and their optical properties. *Nanoscale Res. Lett.* **2013**, *46*, 8. [[CrossRef](#)]
35. Basavaraj, B.; Metri, P.G.; Shweta, G.C.; Sannakki, B. Complex Optical Studies on Conducting Polypyrrole Doped with ZnO Nanoparticles. *Macromol. Symp.* **2020**, *393*, 2000096. [[CrossRef](#)]
36. Botewad, S.N.; Pahurkar, V.G.; Muley, G.G.; Gaikwad, D.K.; Bodkhe, G.A.; Shirsat, M.D.; Pawar, P.P. PANI-ZnO Cladding-Modified Optical Fiber Biosensor for Urea Sensing Based on Evanescent Wave Absorption. *Front. Mater.* **2020**, *7*, 184. [[CrossRef](#)]
37. Mahalakshmi, S.; Hema, V.; Vijaya, P.P. In Vitro Biocompatibility and Antimicrobial activities of Zinc Oxide Nanoparticles (ZnO NPs) Prepared by Chemical and Green Synthetic Route—A Comparative Study. *BioNanoScience* **2020**, *10*, 112–121. [[CrossRef](#)]
38. Nagaraju, G.; Udayabhanu; Shivaraj; Prashanth, S.A.; Shastri, M.; Yathish, K.V.; Anupama, C.; Rangapp, D. Electrochemical heavy metal detection, photocatalytic, photoluminescence, biodiesel production and antibacterial activities of Ag–ZnO nanomaterial. *Mater. Res. Bull.* **2017**, *94*, 54–63. [[CrossRef](#)]
39. Rahman, M.M.; Alam, M.M.; Asiri, A.M.; Uddin, J. Assessment of Melamine in Different Water Samples with ZnO-doped Co₃O₄ Nanoparticles on a Glassy Carbon Electrode by Differential Pulse Voltammetry. *Chem. Asian J.* **2021**, *16*, 1820–1831. [[CrossRef](#)]
40. Rahman, M.M.; Alam, M.M.; Alfaifi, S.Y.M.; Asiri, A.M.; Ali, M.M. Sensitive Detection of Thiourea Hazardous Toxin with Sandwich-Type Nafion/CuO/ZnO Nanospikes/Glassy Carbon Composite Electrodes. *Polymers* **2021**, *13*, 3998. [[CrossRef](#)]
41. Elgrishi, N.; Rountree, K.J.; McCarthy, B.D.; Rountree, E.S.; Eisenhart, T.T.; Dempsey, J.L. A Practical Beginner's Guide to Cyclic Voltammetry. *J. Chem. Educ.* **2018**, *95*, 197–206. [[CrossRef](#)]
42. Zhang, Y.; Wu, L.; Lei, W.; Xia, X.; Xia, M.; Hao, Q. Electrochemical determination of 4-nitrophenol at polycarbazole/N-doped graphene modified glassy carbon electrode. *Electrochim. Acta* **2014**, *146*, 568–576. [[CrossRef](#)]
43. Rajkumar, C.; Veerakumar, P.; Chen, S.M.; Thirumalraj, B.; Lin, K.C. Ultrathin Sulfur-Doped Graphitic Carbon Nitride Nanosheets As Metal-Free Catalyst for Electrochemical Sensing and Catalytic Removal of 4-Nitrophenol. *ACS Sustain. Chem. Eng.* **2018**, *6*, 16021–16031. [[CrossRef](#)]
44. Ahmad, N.; Alam, M.; Wahab, R.; Ahmad, J.; Ubaidullah, M.; Ansari, A.A.; Alotaibi, N.M. Synthesis of NiO–CeO₂ nanocomposite for electrochemical sensing of perilous 4-nitrophenol. *J. Mater. Sci. Mater.* **2019**, *30*, 17643–17653. [[CrossRef](#)]
45. Vinoth, S.; Sampathkumar, P.; Giribabu, K.; Pandikumar, A. Ultrasonically assisted synthesis of barium stannate incorporated graphitic carbon nitride nanocomposite and its analytical performance in electrochemical sensing of 4-nitrophenol. *Ultrason. Sonochem.* **2020**, *62*, 104855. [[CrossRef](#)]
46. Tang, Y.; Huang, R.; Liu, C.; Yang, S.; Lu, Z.; Luo, S. Electrochemical detection of 4-nitrophenol based on a glassy carbon electrode modified with a reduced graphene oxide/Au nanoparticle composite. *Anal. Methods.* **2013**, *5*, 5508–5514. [[CrossRef](#)]
47. Ding, Q.; Kang, Z.; Cao, L.; Lin, M.; Lin, H.; Yang, D.P. Conversion of waste eggshell into difunctional Au/CaCO₃ nanocomposite for 4-Nitrophenol electrochemical detection and catalytic reduction. *Appl. Surf. Sci.* **2020**, *510*, 145526. [[CrossRef](#)]
48. Peng, D.; Zhang, J.; Qin, D.; Chen, J.; Shan, D.; Lu, X. An electrochemical sensor based on polyelectrolyte-functionalized graphene for detection of 4-nitrophenol. *J. Electroanal. Chem.* **2014**, *734*, 1–6. [[CrossRef](#)]
49. Zeng, Y.; Zhou, Y.; Zhou, T.; Shi, G. A novel composite of reduced graphene oxide and molecularly imprinted polymer for electrochemical sensing 4-nitrophenol. *Electrochim. Acta* **2014**, *130*, 504–511. [[CrossRef](#)]
50. Li, J.; Kuang, D.; Feng, Y.; Zhang, F.; Xu, Z.; Liu, M. A graphene oxide-based electrochemical sensor for sensitive determination of 4-nitrophenol. *J. Hazard. Mater.* **2012**, *201–202*, 250–259. [[CrossRef](#)]
51. Zhang, C.; Govindaraju, S.; Giribabu, K.; Huh, Y.S.; Yun, K. AgNWs-PANI nanocomposite based electrochemical sensor for detection of 4-nitrophenol. *Sens. Actuators B Chem.* **2017**, *252*, 616–623. [[CrossRef](#)]
52. Rahman, M.M.; Alam, M.M.; Asiri, A.M. 2-Nitrophenol sensor-based wet-chemically prepared binary doped Co₃O₄/Al₂O₃ nanosheets by an electrochemical approach. *RSC Adv.* **2018**, *8*, 960–970. [[CrossRef](#)]
53. Alam, M.M.; Asiri, A.M.; Rahman, M.M. Electrochemical detection of 2-nitrophenol with BaO nanorods modified glassy carbon electrode. *Chemistry Asian J.* **2021**, *16*, 1475–1485. [[CrossRef](#)]
54. Rahman, M.M.; Alam, M.M.; Hussain, M.M.; Asiri, A.M.; Zayed, M.E.M. Hydrothermally prepared Ag₂O/CuO nanomaterial for an efficient chemical sensor development for environmental remediation. *Environ. Nanotechnol. Monit. Manag.* **2018**, *10*, 1–9. [[CrossRef](#)]

55. Abdel-Latif, I.A.; Singh, C.; Joshi, R.; Singh, J.; Gismelssed, A.; Alam, M.M.; Al-Hajji, L.A.; Ismail, A.A.; Faisal, M.; Asiri, A.M.; et al. Fabrication of Highly Sensitive 4-Nitrophenol Sensor and Photocatalytic Performance of Multifunctional $Ba_{0.5}Sr_{0.5}Co_xHf_xFe_{12-2x}O_{19}$ Ferrite. *Mater. Chem. Phys.* **2022**, *288*, 126396. [[CrossRef](#)]
56. Subhan, M.A.; Saha, P.C.; Ahmed, J.; Asiri, A.M.; Al-Mamun, M.; Rahman, M.M. Development of an ultra-sensitive para-nitrophenol sensor using tri-metallic oxide $MoO_2.Fe_3O_4.CuO$ nanocomposites. *Mater. Adv.* **2020**, *1*, 2831–2839. [[CrossRef](#)]
57. Rahman, M.M.; Marwani, H.M.; Algethami, F.K.; Asiri, A.M.; Hameed, S.A.; Alhogbi, B. Ultra-sensitive p-nitrophenol sensing performances based on various Ag_2O conjugated carbon material composites. *Environ. Nanotechnol. Monit. Manag.* **2017**, *8*, 73–82.
58. Rahman, M.M.; Sheikh, T.A.; Asiri, A.M.; Alamry, K.A.; Hasnat, M.A. Fabrication of ultra-sensitive para-nitrophenol sensor based on facile Zn-doped Er_2O_3 nano-composites by electrochemical approach. *Anal. Methods* **2020**, *12*, 3470–3483. [[CrossRef](#)]
59. Uddin, M.T.; Alam, M.M.; Asiri, A.M.; Rahman, M.M.; Toupance, T.; Islam, M.A. Electrochemical detection of 2-nitrophenol using heterostructure ZnO/RuO₂ nanoparticle modified glassy carbon electrode. *RSC Adv.* **2020**, *10*, 122–132. [[CrossRef](#)]
60. Khan, A.; Khan, A.A.P.; Rahman, M.M.; Asiri, A.M.; Inamuddin; Alamry, K.A.; Hamed, S.A. Preparation and characterization of PANI@G/CWO nanocomposite for enhanced 2-nitrophenol sensing. *Appl. Surface Sci.* **2017**, *433*, 696–704. [[CrossRef](#)]
61. Alam, M.K.; Rahman, M.M.; Abbas, M.; Torati, S.R.; Asiri, A.M.; Kim, D.; Kim, C.G. Ultra-sensitive 2-nitrophenol detection based on reduced graphene oxide/ZnO nanocomposites. *J. Electroanal. Chem.* **2017**, *788*, 66–73. [[CrossRef](#)]
62. Hussain, M.M.; Rahman, M.M.; Asiri, A.M. Efficient 2-nitrophenol chemical sensor development based on Ce_2O_3 nanoparticles decorated CNT nanocomposites for environmental safety. *PLoS ONE* **2016**, *11*, e0166265. [[CrossRef](#)] [[PubMed](#)]
63. Khan, S.B.; Rahman, M.M.; Akhtar, K.; Asiri, A.M.; Rub, M.A. Nitrophenol Chemi-Sensor and Active solar photocatalyst based on Spinel Hetaerolite Nanoparticles. *PLoS ONE* **2014**, *9*, e85290. [[CrossRef](#)] [[PubMed](#)]
64. Wang, B.; He, Q.; Li, G.; Long, Y.; Zhang, G.; Liu, H.; Liu, J. Sensitive Determination of Trace 4-Nitrophenol in Ambient Environment Using a Glassy Carbon Electrode Modified with Formamide-Converted Nitrogen-Doped Carbon Materials. *Int. J. Mol. Sci.* **2022**, *23*, 12182. [[CrossRef](#)] [[PubMed](#)]